METAMATERIAL-ENHANCED VIBRATIONAL CIRCULAR DICHROISM FOR MID-INFRARED SPECTROSCOPIC NANOSENSORS

Cheng Xu[1,2], Zhihao Ren[1,2], Hong Zhou[1,2], Jingkai Zhou[1], Chong Pei Ho[2], Nan Wang[2], and Chengkuo Lee[1,]*

[1]Department of Electrical and Computer Engineering, National University of Singapore, Singapore 117576, Singapore and

[2]Intisittute of Microelectronics (IME), Agency for Science, Technology and Research, Singapore 138634, Singapore

ABSTRACT

Vibrational circular dichroism (VCD) spectroscopy plays an important role in molecule sensing. However, the main limitation is the weak molecule signals (~10^{-5}). In this work, we propose mid-infrared chiral metamaterials (MIRCMs) to demonstrate an enhanced VCD platform. Guided by temporal coupled-mode theory, our proposed chiral metamaterials break both the in-plane and the out-of-plane symmetry to create a larger circular dichroism signal. Leveraging such a platform, we demonstrated a 6-magnitude enhancement compared with traditional VCD spectroscopy. Moreover, we for the first time demonstrate the enhanced selective sensing of chiral mixtures, expanding the VCD spectroscopy for stereochemistry and clinical diagnosis applications.

KEYWORDS

Chiral light-matter interaction, vibrational circular dichroism, protein secondary structure sensing, chiral metamaterials

INTRODUCTION

Circular dichroism (CD) describes the absorption difference towards circularly polarized light[1]. Therefore, CD spectroscopy has been widely used for chiral molecule sensing applications[2]. The main limitation is the lack of dimensionality of the sensing signal, where the chiral-induced wavelength shift is usually the only effective information. Hence, it is usually difficult for traditional UV-visible CD spectroscopy to handle multiple-molecule sensing processes, especially chiral mixtures. One of the methods to solve this problem is to extend to the mid-infrared (MIR) range, where the vibrational transition of molecules can be leveraged as another dimension of the sensing signal[3], called vibrational circular dichroism (VCD). However, the natural VCD signal is very weak, which is only around 10^{-5} level[4]. Regarding the problem, many works designed nanostructures to utilize strong near-field confinement to achieve enhanced molecular signal, such as photonic crystals[5]–[8], plasmonic metamaterials[9]–[15], and waveguide sensors[16]–[22]. Moreover, geometric chiral nanostructures can also present chiroptical response in the MIR range, which are widely used for chiral molecule sensing[23], polarization detection applications[24]–[26]. However, there lack of a design

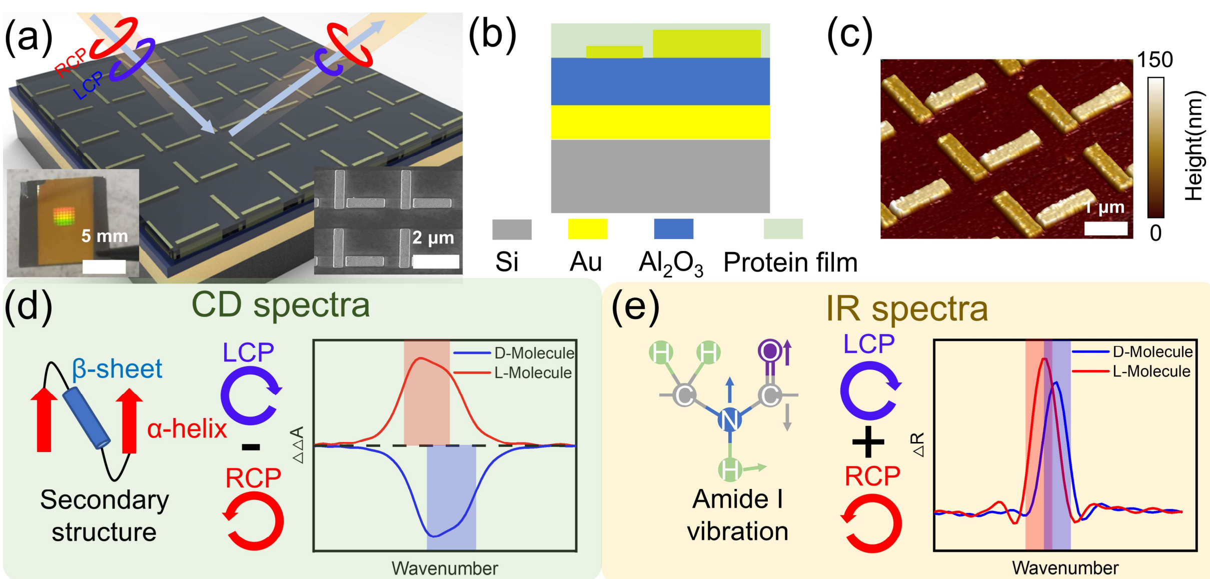

Figure 1: (a) Schematic drawing of proposed MIRCMs. The metamaterials are composed of MIM structure, where the LCP and RCP lights are reflected with different reflection. (b) Building blocks and the materials used of the metamaterials. (c) Atomic force microscope (AFM) image shows the difference thickness of the two nanorods that break the out-of-plane symmetry. (d) Proposed protein secondary structure sensing process of CD spectra, opposite CD signal is detected by subtracting the reflected LCP and RCP lights. (e) Proposed amide I vibration transition sensing process of IR spectra. The absorption peaks illustrate the IR fingerprint of the molecules.

framework to reveal the working mechanism for the nanostructure design. Besides, none of the existing works have demonstrated chiral mixture sensing using enhanced VCD spectroscopy so far, which hinders the potential of this valuable technology.

In this work, we propose mid-infrared chiral metamaterials (MIRCMs) platform to enhance the weak VCD signal. Such chiral metamaterials are composed of symmetry-breaking nanorods that can generate reflected CD signals. We demonstrate a 6-magnitude enhancement VCD signal compared with traditional spectroscopy. Furthermore, we for the first time distinguish protein secondary structures in a mixture using an enhanced VCD platform, demonstrating a label-free method to detect molecular chirality in a complex environment.

RESULTS AND DISCUSSION

Working mechanism of proposed MIRCMs

Figure 1 shows the working mechanisms of our proposed chiral metamaterials. The schematic, photograph, and scanning electron microscope (SEM) images are shown in Figure 1 (a), (b). The vertical structure is composed of metal-insulator-metal (MIM) layer, where the thicknesses of the bottom metal and middle insulator are 100 nm and 200 nm, respectively. We break the out-of-plane symmetry by varying the thicknesses of the nanorods, which is characterized using AFM, as shown in Figure 1(c). Leveraging this platform, we use two proteins, BSA and β-lactoglobulin for the demonstration of the enhanced sensing process. The two proteins both contain secondary structures α-helix and β-sheet with a different ratio, which can present different chiroptical responses, as shown in Figure 1(d). Besides, the sensitive amide I vibration can also be detected in the range from 1600 cm^{-1} to 1700 cm^{-1}, as shown in Figure 1(e). Our platform leverages the enhanced VCD signals, enabling the detection of secondary structures are amide I vibrations simultaneously.

Device optimization framework

The design framework can be comprehended by a two-port temporal coupled-mode theory (TCMT):

$$\frac{d}{dt}\begin{pmatrix}P_x\\P_y\end{pmatrix}=j\begin{pmatrix}\omega_x' & -\xi\\-\xi & \omega_y'\end{pmatrix}\begin{pmatrix}P_x\\P_y\end{pmatrix}+\begin{pmatrix}\kappa_x & 0\\0 & \kappa_y\end{pmatrix}\begin{pmatrix}s_x^+\\s_y^+\end{pmatrix} \quad (1)$$

$$\omega_x'=\omega_x+j(\gamma_{rx}+\gamma_{ax}) \quad (2)$$

$$\omega_y'=\omega_y+j(\gamma_{ry}+\gamma_{ay}) \quad (3)$$

$$\begin{pmatrix}s_x^-\\s_y^-\end{pmatrix}=\begin{pmatrix}-1 & 0\\0 & -1\end{pmatrix}\begin{pmatrix}s_x^+\\s_y^+\end{pmatrix}+\begin{pmatrix}\kappa_x & 0\\0 & \kappa_y\end{pmatrix}\begin{pmatrix}P_x\\P_y\end{pmatrix} \quad (4)$$

where the two orthogonal resonant modes P_x and P_y refer to the plasmonic nanorods positioned along x and y axis. The resonant frequencies are denoted as ω_x' and ω_y', which are dependent on the absorption loss γ_a and radiative loss γ_r. The mode coupling coefficient is written as far field coefficient κ_x, κ_y, and near field coupling coefficient ξ. The detailed relationship between the coefficients is shown in Figure 2(a). By solving the equations from (1) to (4), we conclude that the reflective circular dichroism R_{CD} is proportional to the near field coupling coefficient ξ and loss ratio $\Delta\gamma_a/\gamma_r$, determined as $\Delta\gamma_a/\gamma_r=\gamma_{ax}/\gamma_{rx}-\gamma_{ay}/\gamma_{ry}$. We further calculate and map the parameters, shown in Figure 2(b). From the results, to achieve a larger CD, the loss ratio

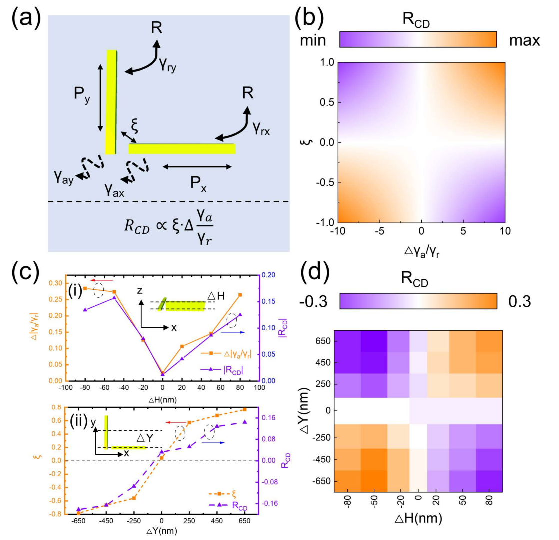

Figure 2: (a) Schematic drawing of the TCMT model. (b) Calculation of the R_{CD} with varied ξ and $\Delta\gamma_a/\gamma_r$. The color bar shows the normalized CD response. (c) Extracted ξ and $\Delta\gamma_a/\gamma_r$ for nanorods with different (i) ΔH and (ii) ΔY. (d) Simulated CD results with varied ΔH and ΔY.

between the orthogonal modes as well as the near-field coupling strengths should be increased. To fulfill such requirements, we use different nanorod thicknesses (ΔH) to enlarge the absorption loss difference while changing the position of the x-oriented nanorod (ΔY) to create hotspots for stronger near-field coupling. The extracted parameters for such structural optimization are shown in Figure 2(c). We further simulate the geometric parameters using Lumerical finite-difference time-domain (FDTD) solver, shown in Figure 2(d). The results agree well with the calculation results shown in Figure 2(b), indicating the reasonable design framework of breaking both in-plane symmetry ΔY and out-of-plane symmetry ΔH.

Enhanced VCD measurement results

We fabricate our device through a two-step e-beam lithography (EBL) process. A thermal evaporation and lift-off process is followed to construct nanorods. The different thickness ΔH is fixed as -50 nm. We choose right-handed chiral (RC) metamaterial, left-handed (LC) metamaterial, and achiral (AC) metamaterial for sensing demonstration, as shown in Figure 3. From the simulation results shown in Figure 3(a), 3(b), AC metamaterials have the largest electric field intensity, while RC and LC metamaterials have larger optical chiral field enhancement, which is defined as $C=-\varepsilon_0\omega(\mathbf{E}^*\bullet\mathbf{B})/2$, where ε_0 is the permittivity in vacuum, ω is the angular frequency, **E** and **B** are the electric field and magnetic field, respectively. We use C/C_0 to present the enhancement optical chirality, where C_0 is the optical chiral field in free space. Based on the simulation results, we use AC for IR sensing demonstration, the results are shown in Figure 3(c). The two absorption peaks of β-lactoglobulin and BSA indicate the enhanced IR absorption peaks of amide II and amide I, respectively. We further characterize the VCD signal of the amide I peak, shown in Figure 3(d). The ΔΔA means the absorption difference of ΔR between LCP and RCP illuminance. We can observe

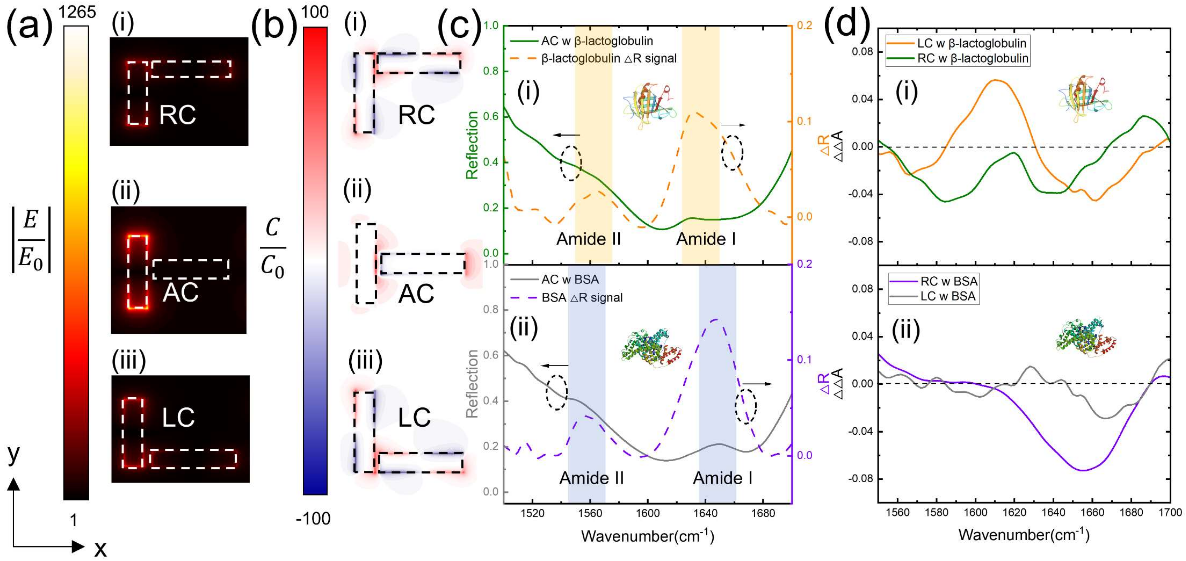

Figure 3: (a) and (b) show the electrical field and optical chiral field of RC, LC, and AC metamaterial. (c) Enhanced IR absorption signal of (i) β-lactoglobulin and (ii) BSA on AC metamaterial. (d) Enhanced CD signal of (i) β-lactoglobulin and (ii) BSA on LC and RC metamaterials.

that the LC metamaterial selectively amplifies the ΔΔA signal of β-lactoglobulin, while the RC metamaterial shows more BSA signal enhancement. The results indicate that β-lactoglobulin contains more β-sheet structures, while BSA contains more α-helix structures. Moreover, these enhanced protein signals show 6-magnitude enhancement compared with traditional VCD spectroscopy[4].

Characterization of sensitivity and mixture sensing

We further measure the sensitivity and mixture sensing process, shown in Figure 4. We diluted the protein solutions with varied concentrations and measured their VCD signals of them, as shown in Figure 4(a), 4(b). The highest sensitivity for BSA is the enhanced IR absorption signal that reaches 14.3 %/μM, with a CD sensitivity of 7.6 %/μM. Besides, we also demonstrate mixture sensing with different ratios from 1:4 to 4:1, as shown in Figure 4(c), 4(d). Although the IR absorption spectra could distinguish two amide I absorption peaks at 1630 cm^{-1} and 1650 cm^{-1}, it's still difficult to tell the ratio. Fortunately, with CD spectra, more information can be provided from different optical chirality, while the differential signal can also illustrate the ratio difference. This demonstration expands the vibrational transitions to the CD spectra and solves the signal overlap problem for IR spectra.

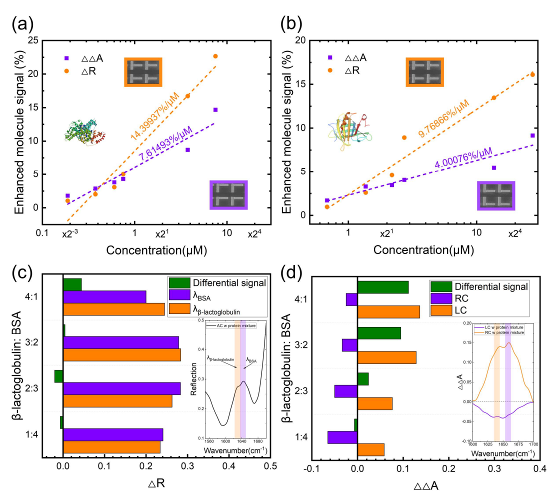

Figure 4: (a) and (b) show the VCD sensitivity of two proteins with varied concentrations. (c) and (d) show the IR and CD sensing signal of protein mixtures.

CONCLUSION

In this work, we demonstrate a chiral metamaterial platform for enhanced VCD sensing. The design framework is theoretically explained using the TCMT method. We use proteins for sensing demonstration, and the sensitivity shows a 6-magnitude enhancement. Besides, we also for the first time demonstrate the sensing process of chiral mixtures using the enhanced VCD platform. Such demonstration expands more potentiality for VCD spectroscopy and opens a new avenue for biomedical applications.

ACKNOWLEDGEMENTS

This work was supported by A18A5b0056, A-0005947-20-00, A-0009520-01-00, and NRF-CRP15-2015-02.

REFERENCES

[1] J. Mun *et al.*, "Electromagnetic chirality: from fundamentals to nontraditional chiroptical phenomena," *Light Sci. Appl.*, vol. 9, no. 1, p. 139, Dec. 2020.

[2] L. A. Warning, A. R. Miandashti, L. A. McCarthy, Q. Zhang, C. F. Landes, and S. Link, "Nanophotonic Approaches for Chirality Sensing," *ACS Nano*, vol. 15, no. 10, pp. 15538–15566, Oct. 2021.

[3] T. A. Keiderling, “Structure of Condensed Phase Peptides: Insights from Vibrational Circular Dichroism and Raman Optical Activity Techniques,” *Chem. Rev.*, vol. 120, no. 7, pp. 3381–3419, Apr. 2020.

[4] V. Baumruk and T. A. Keiderling, “Vibrational circular dichroism of proteins in water solution,” *J. Am. Chem. Soc.*, vol. 115, no. 15, pp. 6939–6942, Jul. 1993.

[5] Y. Chang *et al.*, “Development of triboelectric-enabled tunable Fabry-Pérot photonic-crystal-slab filter towards wearable mid-infrared computational spectrometer,” *Nano Energy*, vol. 89, p. 106446, Nov. 2021.

[6] Y. Chang *et al.*, “All-Dielectric Surface-Enhanced Infrared Absorption-Based Gas Sensor Using Guided Resonance,” *ACS Appl. Mater. Interfaces*, vol. 10, no. 44, pp. 38272–38279, Nov. 2018.

[7] Q. Qiao, C. Peng, J. Xia, C. Lee, and G. Zhou, “Ultra-small photonic crystal (PhC)-based test tool for gas permeability of polymers,” *Opt. Express*, vol. 27, no. 24, 2019.

[8] X. Liu *et al.*, “Progress of optomechanical micro/nano sensors: a review,” *International Journal of Optomechatronics*, vol. 15, no. 1. Taylor & Francis, pp. 120–159, Jan. 01, 2021.

[9] H. Zhou, Z. Ren, C. Xu, L. Xu, and C. Lee, “MOF/Polymer-Integrated Multi-Hotspot Mid-Infrared Nanoantennas for Sensitive Detection of CO2 Gas,” *Nano-Micro Lett.*, vol. 14, no. 1, p. 207, Dec. 2022.

[10] Z. Ren, Z. Zhang, J. Wei, B. Dong, and C. Lee, “Wavelength-multiplexed hook nanoantennas for machine learning enabled mid-infrared spectroscopy,” *Nat. Commun.*, vol. 13, no. 1, p. 3859, Jul. 2022.

[11] H. Zhou, D. Li, Z. Ren, X. Mu, and C. Lee, “Loss-induced phase transition in mid-infrared plasmonic metamaterials for ultrasensitive vibrational spectroscopy,” *InfoMat*, vol. 4, no. 12, pp. 1–18, Dec. 2022.

[12] H. Zhou, L. Xu, Z. Ren, J. Zhu, and C. Lee, “Machine learning-augmented surface-enhanced spectroscopy toward next-generation molecular diagnostics,” *Nanoscale Adv.*, vol. 5, no. 3, pp. 538–570, 2023.

[13] J. Wei *et al.*, “Ultrasensitive Transmissive Infrared Spectroscopy via Loss Engineering of Metallic Nanoantennas for Compact Devices,” *ACS Appl. Mater. Interfaces*, vol. 11, no. 50, pp. 47270–47278, Dec. 2019.

[14] J. Xu *et al.*, “Nanometer-Scale Heterogeneous Interfacial Sapphire Wafer Bonding for Enabling Plasmonic-Enhanced Nanofluidic Mid-Infrared Spectroscopy,” *ACS Nano*, vol. 14, no. 9, pp. 12159–12172, Sep. 2020.

[15] H. Zhou, D. Li, X. Hui, and X. Mu, “Infrared metamaterial for surface-enhanced infrared absorption spectroscopy: pushing the frontier of ultrasensitive on-chip sensing,” *Int. J. Optomechatronics*, vol. 15, no. 1, pp. 97–119, Jan. 2021.

[16] J. Zhou, Z. Zhang, B. Dong, Z. Ren, W. Liu, and C. Lee, “Midinfrared Spectroscopic Analysis of Aqueous Mixtures Using Artificial-Intelligence-Enhanced Metamaterial Waveguide Sensing Platform,” *ACS Nano*, vol. 17, no. 1, pp. 711–724, Jan. 2023.

[17] W. Liu *et al.*, “Larger-Than-Unity External Optical Field Confinement Enabled by Metamaterial-Assisted Comb Waveguide for Ultrasensitive Long-Wave Infrared Gas Spectroscopy,” *Nano Lett.*, vol. 22, no. 15, pp. 6112–6120, Aug. 2022.

[18] W. Liu *et al.*, “Suspended silicon waveguide platform with subwavelength grating metamaterial cladding for long-wave infrared sensing applications,” *Nanophotonics*, vol. 10, no. 7, pp. 1861–1870, May 2021.

[19] Y. Ma, Y. Chang, B. Dong, J. Wei, W. Liu, and C. Lee, “Heterogeneously Integrated Graphene/Silicon/Halide Waveguide Photodetectors toward Chip-Scale Zero-Bias Long-Wave Infrared Spectroscopic Sensing,” *ACS Nano*, vol. 15, no. 6, pp. 10084–10094, Jun. 2021.

[20] Y. Chang, B. Dong, Y. Ma, J. Wei, Z. Ren, and C. Lee, “Vernier effect-based tunable mid-infrared sensor using silicon-on-insulator cascaded rings,” *Opt. Express*, vol. 28, no. 5, p. 6251, 2020.

[21] B. Dong *et al.*, “Biometrics-protected optical communication enabled by deep learning-enhanced triboelectric/photonic synergistic interface,” *Sci. Adv.*, vol. 8, no. 3, Jan. 2022.

[22] X. Liu *et al.*, “MEMS enabled suspended silicon waveguide platform for long-wave infrared modulation applications,” *Int. J. Optomechatronics*, vol. 16, no. 1, pp. 42–57, Dec. 2022.

[23] A. Vázquez-Guardado and D. Chanda, “Superchiral Light Generation on Degenerate Achiral Surfaces,” *Phys. Rev. Lett.*, vol. 120, no. 13, p. 137601, Mar. 2018.

[24] J. Wei *et al.*, “Geometric filterless photodetectors for mid-infrared spin light,” *Nat. Photonics*, vol. 17, no. 2, pp. 171–178, Feb. 2022.

[25] J. Wei, C. Xu, B. Dong, C. W. Qiu, and C. Lee, “Mid-infrared semimetal polarization detectors with configurable polarity transition,” *Nat. Photonics*, vol. 15, no. 8, pp. 614–621, Aug. 2021.

[26] Q. Li, Z. Li, and J. Meng, “Pyro-phototronic effect enhanced self-powered photodetector,” *Int. J. Optomechatronics*, vol. 16, no. 1, pp. 1–17, Dec. 2022.

CONTACT

*C. Lee, tel: +65-65165865; elelc@nus.edu.sg